



# The influence of deep convection on HCHO and H<sub>2</sub>O<sub>2</sub> in the upper troposphere over Europe

Heiko Bozem<sup>1,a</sup>, Andrea Pozzer<sup>1</sup>, Hartwig Harder<sup>1</sup>, Monica Martinez<sup>1</sup>, Jonathan Williams<sup>1</sup>, Jos Lelieveld<sup>1</sup>, and Horst Fischer<sup>1</sup>

<sup>1</sup>Atmospheric Chemistry Department, Max Planck Institute for Chemistry, P.O. Box 3060, 55020 Mainz, Germany

<sup>a</sup>now at: Institute for Atmospheric Physics, Johannes Gutenberg University, Mainz, Germany

Correspondence to: Heiko Bozem (bozemh@uni-mainz.de)

Received: 17 February 2017 – Discussion started: 16 March 2017

Revised: 9 August 2017 – Accepted: 22 August 2017 – Published: 6 October 2017

**Abstract.** Deep convection is an efficient mechanism for vertical trace gas transport from Earth's surface to the upper troposphere (UT). The convective redistribution of short-lived trace gases emitted at the surface typically results in a C-shaped profile. This redistribution mechanism can impact photochemical processes, e.g. ozone and radical production in the UT on a large scale due to the generally longer lifetimes of species like formaldehyde (HCHO) and hydrogen peroxide (H<sub>2</sub>O<sub>2</sub>), which are important HO<sub>x</sub> precursors (HO<sub>x</sub> = OH + HO<sub>2</sub> radicals). Due to the solubility of HCHO and H<sub>2</sub>O<sub>2</sub> their transport may be suppressed as they are efficiently removed by wet deposition. Here we present a case study of deep convection over Germany in the summer of 2007 within the framework of the HOOVER II project. Airborne in situ measurements within the in- and outflow regions of an isolated thunderstorm provide a unique data set to study the influence of deep convection on the transport efficiency of soluble and insoluble trace gases. Comparing the in- and outflow indicates an almost undiluted transport of insoluble trace gases from the boundary layer to the UT. The ratios of out : inflow of CO and CH<sub>4</sub> are  $0.94 \pm 0.04$  and  $0.99 \pm 0.01$ , respectively. For the soluble species HCHO and H<sub>2</sub>O<sub>2</sub> these ratios are  $0.55 \pm 0.09$  and  $0.61 \pm 0.08$ , respectively, indicating partial scavenging and washout. Chemical box model simulations show that post-convection secondary formation of HCHO and H<sub>2</sub>O<sub>2</sub> cannot explain their enhancement in the UT. A plausible explanation, in particular for the enhancement of the highly soluble H<sub>2</sub>O<sub>2</sub>, is degassing from cloud droplets during freezing, which reduces the retention coefficient.

## 1 Introduction

Deep convection can transport trace gases from the boundary layer to the upper troposphere (UT) on timescales of hours, thus establishing an efficient mechanism for vertical redistribution of trace gases in the troposphere (Gidel, 1983; Chatfield and Crutzen, 1984; Dickerson et al., 1987; Garstang et al., 1988; Pickering et al., 1989; Scala et al., 1990; Lelieveld and Crutzen, 1994; Barth et al., 2015). Especially at mid-latitudes, strong zonal winds in the UT accelerate the long-range transport of convectively advected trace gases whose sources are in the planetary boundary layer. Thus, reactive gases like nitrogen oxides (NO<sub>x</sub> = NO + NO<sub>2</sub>) and nitrogen compounds that act as NO<sub>x</sub> reservoir species like volatile organic compounds (VOCs), oxygenated VOCs and carbon monoxide (CO), which have extended lifetimes in the UT, can be transported over long distances, thus influencing the atmospheric composition and chemistry at a distance from the sources (Dickerson et al., 1987; Pickering et al., 1996; Jonquière and Marenco, 1998; Ridley et al., 2004; Bertram et al., 2007; Jaeglé, 2007).

The uplift of ozone precursors by deep convection and the addition of lightning produced NO<sub>x</sub> leads to enhanced photochemical ozone production downwind of thunderstorms (Bozem et al., 2017, and references therein). While insoluble species are efficiently transported to the UT via convection, soluble species are scavenged by cloud and rain droplets, with subsequent removal by precipitation (Wang and Crutzen, 1995; Crutzen and Lawrence, 2000). Nevertheless, recent observations have shown that highly soluble species can also reach the UT via deep convection, most likely due to incomplete removal of these species during pre-

precipitation events (Crutzen and Lawrence, 2000; Marie et al., 2000; Barth et al., 2001, 2016; Yin et al., 2002; Borbon et al., 2012; Bela et al., 2016; Fried et al., 2016). Considerable uncertainty remains with respect to the processes that control the concentrations of soluble species in the outflow of deep convection. Crutzen and Lawrence (2000) emphasize the role of post-convective local photochemical production leading to enhancements of soluble species in the UT, while the study of Barth et al. (2001) identifies dynamical and microphysical processes as the main causes for incomplete removal within clouds. Barth et al. (2001) used a 3-D cloud resolving model to study transport in a mid-latitude storm. Their assumption of incomplete retention of soluble trace gases during freezing of liquid cloud droplets was shown to contribute significantly to transport of soluble species like hydrogen peroxide ( $\text{H}_2\text{O}_2$ ) to the outflow in the UT, while the assumption of maximum retention both in liquid and ice particles leads to a complete scavenging of  $\text{H}_2\text{O}_2$ . Based on a 1-D-model study Marie et al. (2000) show that incomplete scavenging of  $\text{H}_2\text{O}_2$  and other species can lead to significant enhancement in the outflow of deep convection. Besides  $\text{H}_2\text{O}_2$ , formaldehyde (HCHO) enhancement was also observed in the outflow of deep convection (Prather and Jacob, 1997; Cohan et al., 1999; Stickler et al., 2006; Fried et al., 2008; Borbon et al., 2012). This may be due to transport from the source region (boundary layer) or to secondary production from convectively transported HCHO precursors like methanol ( $\text{CH}_3\text{OH}$ ), acetone ( $\text{CH}_3\text{COCH}_3$ ), acetaldehyde ( $\text{CH}_3\text{CHO}$ ) and methylhydroperoxide ( $\text{CH}_3\text{OOH}$ ) (Prather and Jacob, 1997; Fried et al., 2008), which are generally less soluble than HCHO. Stickler et al. (2006) pointed out that increased NO concentrations due to lightning enhances the HCHO production in the convective outflow. Recently, results from the Deep Convective Clouds and Chemistry (DC3) field campaign (Barth et al., 2015) indicate that, to reproduce the observations, zero ice retention has to be assumed for HCHO and  $\text{H}_2\text{O}_2$ , leading to their incomplete removal by precipitation (Barth et al., 2016; Bela et al., 2016; Fried et al., 2016).

Since both  $\text{H}_2\text{O}_2$  and HCHO are precursors of  $\text{HO}_x$  radicals, transport of these species to the UT in convective clouds has a significant influence on the oxidizing capacity of the UT, since  $\text{HO}_x$  production from photolysis of HCHO and  $\text{H}_2\text{O}_2$  typically exceeds primary OH production from  $\text{O}_3$  photolysis and the subsequent reaction of  $\text{O}(^1\text{D})$  with water vapour (Jaeglé et al., 1997; Prather and Jacob, 1997; Lee et al., 1998; Wang and Prinn, 2000; Marie et al., 2003; Regelin et al., 2013; Lelieveld et al., 2016). Figure 1 illustrates the processes associated with deep convection.

Here we use airborne in situ measurements taken in the in- and outflow regions of an isolated thunderstorm over south-eastern Germany on 19 July 2007 to study the influence of deep convection on the transport efficiency of soluble and insoluble trace gases. Emphasis is given to HCHO, which has a medium solubility described by its Henry's law co-

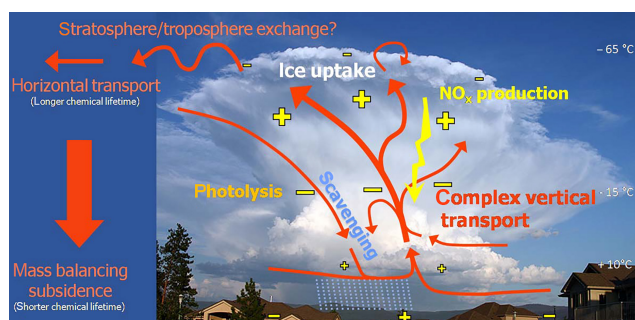


**Figure 1.** Scheme of the relevant characteristics and processes of a thunderstorm cloud.

efficient of  $k_{\text{H}} = 3.2 \times 10^3 \text{ M atm}^{-1}$ , and the highly soluble  $\text{H}_2\text{O}_2$  ( $k_{\text{H}} = 8.2 \times 10^4 \text{ M atm}^{-1}$ ).

## 2 Methods

### 2.1 HOOVER II

The HOOVER project included a total of two measurement campaigns in October 2006 and July 2007, composed of four measurement flights per campaign. From the home airport of Hohn (Germany;  $54.2^\circ \text{N}$ ,  $9.3^\circ \text{E}$ ) regular research flights were performed southbound with a stopover at Bastia in Corsica (France;  $42.2^\circ \text{N}$ ,  $9.29^\circ \text{E}$ ) and northbound with a stopover at Kiruna airport (Sweden  $67.5^\circ \text{N}$ ,  $20.2^\circ \text{E}$ ). The majority of the flights were performed in the UT, while regular profiles were flown in and out of the home and stopover airports, as well as halfway towards the respective destinations over either southern Germany or northern Scandinavia. Additional flights in summer 2007 were directed to the Arctic (Svalbard, Norway;  $78.1^\circ \text{N}$ ,  $15.3^\circ \text{E}$ ) and two flights over central Germany to study the influence of deep convection. On 19 July 2007, an eastward moving mesoscale convective system developed over the southern part of Germany. During a research flight (HOOVER II flight no. 7) out of Baden airport ( $48.4^\circ \text{N}$ ,  $8.4^\circ \text{E}$ ) the in- and outflow of a strong convective cell were probed close to Dresden, the capital of the Free State of Saxony in Germany. Further details about the campaigns can be found in several previous publications (Klippel et al., 2011; Regelin et al., 2013; Bozem et al., 2017).

### 2.2 Observations

During HOOVER, a Learjet 35A from GFD GmbH (Hohn, Germany) was used. The jet aircraft has a range of about 4070 km and a maximum flight altitude of approximately 14 km. In the present configuration, both the range and height maximum were reduced due to the use of two wing pods that housed additional instruments. The instrumentation consisted of a chemiluminescence detector (CLD 790 SR, ECO Physics, Switzerland) for NO,  $\text{NO}_2$  and  $\text{O}_3$  measurements

(Hosaynali Beygi et al., 2011); a set of up- and downward looking  $2\pi$ -steradian filter radiometers for  $j(\text{NO}_2)$  measurements (Meteorologie Consult GmbH, Germany); a quantum cascade laser IR-absorption spectrometer for CO, CH<sub>4</sub> and HCHO measurements (Schiller et al., 2008); a dual enzyme fluorescence monitor (model AL2001 CA peroxide monitor, Aero-Laser GmbH, Germany) to measure H<sub>2</sub>O<sub>2</sub> and organic hydroperoxides (Klippel et al., 2011); a laser induced fluorescence (LIF) instrument for simultaneous measurements of OH and HO<sub>2</sub> (Martinez et al., 2010; Regelin et al., 2013); a non-dispersive IR-absorption instrument (model LI-6262, LI-COR Inc., USA) for CO<sub>2</sub> and H<sub>2</sub>O measurements (Gurk et al., 2008); a proton transfer reaction mass spectrometer (PTR-MS, Ionicon, Austria) for partially-oxidized VOC measurements and a series of canisters for post-flight analysis of non-methane hydrocarbons (Colomb et al., 2006). Details about the instrument performance with respect to time resolution, precision, detection limit and total uncertainty can be found in Klippel et al. (2011), Regelin et al. (2013) and Bozem et al. (2017). For the two species, which are central in the present study, some more details will be given next.

The hydrogen peroxide measurements have a time resolution of 30 s (time for a calibration signal to rise from 10 to 90 % of total reading), a detection limit of 24 pptv (deduced from the  $1\sigma$  reproducibility of in-flight zero air measurements) and a precision of  $\pm 8.3\%$  at 260 pptv (deduced from the standard deviation ( $1\sigma$ ) reproducibility of in-flight calibrations with a liquid standard) resulting in a total uncertainty of  $\pm 13.9\%$  at 260 pptv (Klippel et al., 2011).

The formaldehyde measurements have a time resolution of 30 s (averages over  $\sim 75$  HCHO spectra at a duty cycle of 60 %, while the remainder of the cycle is dedicated to CO and CH<sub>4</sub> measurements), a detection limit of 32 pptv (deduced from the  $1\sigma$  reproducibility of in-flight zero air measurements) and a total uncertainty of  $\pm 9\%$  (Klippel et al., 2011; Schiller et al., 2008). All data used in this study have been averaged over a time interval of 30 s.

### 2.3 Chemistry box model MECCA

In order to estimate photochemical destruction and secondary production of HCHO and H<sub>2</sub>O<sub>2</sub> in the UT after convective injection, the box model MECCA (Module Efficiently Calculating the Chemistry of the Atmosphere) has been used. MECCA uses an extensive chemistry mechanism for gas-phase and liquid-phase chemistry (Sander et al., 2005). It uses the “Kinetic PreProcessor” (KPP), a flexible package for the numerical integration to translate the chemical mechanism into a set of ordinary differential equations (Sandu and Sander, 2006). For atmospheric studies, MECCA is coupled to either the atmospheric chemistry-general circulation model EMAC (ECHAM5/MESSy2 Atmospheric Chemistry, <http://www.messy-interface.org>) or the box model CAABA (Chemistry As A Boxmodel Appli-

cation). The coupling is realized by the MESSy (Modular Earth Submodel System) interface (Jöckel et al., 2006).

For this study, CAABA/MECCA was set up with basic methane, VOC and isoprene chemistry following the Mainz isoprene mechanism (MIM) (Pöschl et al., 2000), a condensed version of the detailed Master Chemical Mechanism (Jenkin et al., 1997). This resulted in a mechanism for tropospheric gas-phase chemistry including 76 species and 153 reactions. Halogen chemistry and liquid phase or heterogeneous chemistry was not included since model calculations were restricted to cloud-free air. Additionally, deposition processes, either wet or dry, were not considered for the same reasons. Equations were solved by a Rosenbrock scheme (Sandu and Sander, 2006). Details of the model set-up and initialization will be discussed in Sect. 3.3.

## 3 Results

### 3.1 Meteorology on 19 July 2007

The meteorological conditions in Europe on 19 July 2007 are shown in Fig. 2. A pool of cold air, associated with a long trough extending from the North Atlantic over the British Isles to the Azores, led to a low pressure system between Spain and Ireland (Fig. 2a). Towards the east, a high pressure ridge extending from North Africa over the eastern Mediterranean, eastern Europe and into Russia started to weaken. Between these systems a strong south-westerly flow was established in the middle and upper troposphere, bringing moist and warm air from Spain to north-western Europe, with a surface frontal zone separating moist, hot air in the south-east from dry, cold air in the north-west (Fig. 2b). Over Germany these conditions led to the development of thunderstorms, favoured by a potentially unstable troposphere with high convective available potential energy (CAPE) values over south-western Germany.

During the night from 18 to 19 July, convective cells developed along a weakening cold front over France, which rapidly developed into a mesoscale convective system (MCS) moving into south-western Germany in the early-morning hours of 19 July. This MCS subsequently travelled in a north-easterly direction accompanied by heavy rain (Fig. 3). Around noon the south-eastern edge of the MCS reached the Nürnberg/Bamberg area. The explosive storm development came with three strong, isolated cells which expanded throughout the whole tropospheric column up to 10 km altitude within 2 hours. The convection in the three cells was accompanied by strong lightning activity. Figure 4 shows the position (Fig. 4a) and intensity (Fig. 4b) of detected lightning flashes on 19 July 2007 between 00:00 and 22:00 UTC. Based on the temporal evolution of the lightning activity (colour code in Fig. 4a), the movement of the MCS over Europe can be traced up to the rapid thunderstorm development over south-eastern Germany (green and yellow points

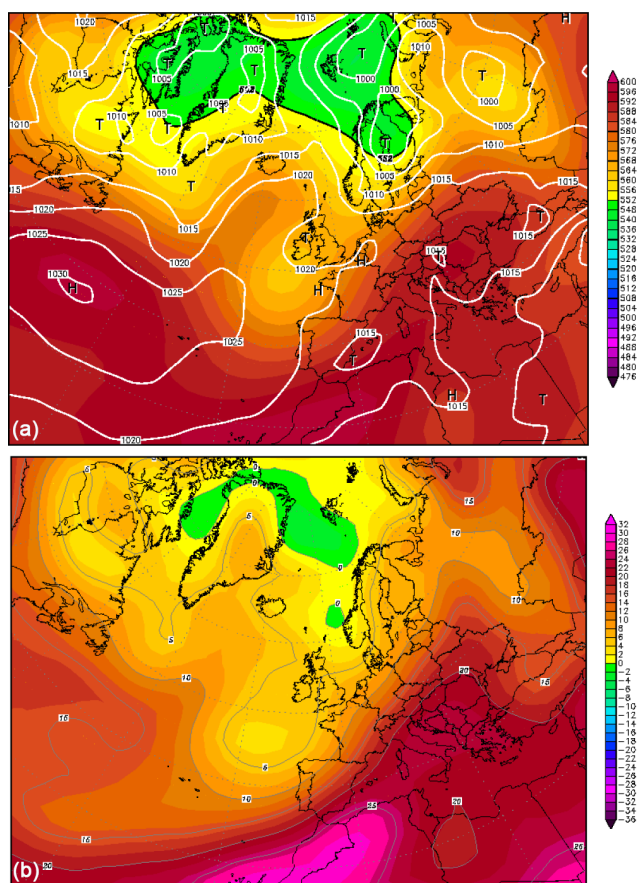


**Figure 2.** NCEP (National Centers for Environmental Prediction) reanalysis data for 19 July 2007. (a) 500 hPa geopotential height (colour scale in m). The white lines mark the surface pressure field (in hPa). (b) Temperature distribution at 850 hPa ( $^{\circ}\text{C}$ ).

in Fig. 4a). During this phase the number of lightning flashes increased to  $50 \text{ min}^{-1}$  (Fig. 4b).

Figure 5a–c shows the RADOLAN (RADar-OnLine-ANEichung) data of the precipitation radar of the German weather service for the time period of rapid development over the Nürnberg/Bamberg area. During the initial storm development (Fig. 5a), from 11:30 to 12:30 UTC, precipitation is observed associated with the MCS. Later on (12:30 to 13:30 UTC; Fig. 5b), the isolated thunderstorm cells, being investigated here, emerged. Superimposed on the figure is the flight track of the Learjet after takeoff from Baaden airport to the UT ahead of the MCS. The precipitation signal from three not fully separated thunderstorm cells in the time interval 13:30–14:30 UTC together with the flight track of the Learjet is shown in Fig. 5c. The strongest cell at the most northerly position with a maximum precipitation intensity of  $30 \text{ mm h}^{-1}$  was intensively probed by the research aircraft, performing measurements around the cell at various altitudes in, above and below the outflow during the final period (14:30 to 15:30 UTC; Fig. 5d). The outflow, which occurred at an altitude of 10.5 km, was identified in-flight by the strong en-

hancements of a number of trace gases (see Sect. 3.2) and sampled for about 5 min. Due to the close proximity of the three cells, the outflow cannot be assigned unambiguously to an individual cell but on-board wind measurements strongly support our interpretation that the outflow originated from the northernmost cell.

The research flight was continued by measurements ahead of the weakening MCS. Around Dresden, descents into the continental boundary layer were flown, followed by ascents to obtain trace gas profiles and to characterize the potential inflow region, spending 15 min in the boundary layer. Although the inflow region cannot be identified unambiguously the storm track and local winds support our interpretation.

### 3.2 Observations

Figure 6 shows a time series of trace gas measurements ( $\text{CH}_3\text{OH}$ ,  $\text{CH}_3\text{COCH}_3$ ,  $\text{HO}_2$ ,  $\text{OH}$ ,  $\text{NO}$ ,  $\text{O}_3$ ,  $\text{H}_2\text{O}_2$ ,  $\text{HCHO}$ ,  $\text{CH}_4$ ,  $\text{CO}$  and flight altitude) from HOOVER flight 7 on 19 July 2007. The first part of the flight was conducted in the wake of the eastward-moving MCS and up-wind of the developing thunderstorm cells. Signatures of convection can be identified during various parts of the flight. The first significant enhancements in  $\text{CO}$  and  $\text{CH}_4$  between 13:00 and 13:10 UTC at an altitude between 7.5 and 8 km were influenced by activity of the MCS that moved over the area earlier during the day. Signatures of recent convection can also be identified from enhancements of  $\text{O}_3$  and  $\text{CH}_3\text{COCH}_3$ , while mixing ratios of shorter-lived species e.g.  $\text{NO}$ ,  $\text{HCHO}$ ,  $\text{H}_2\text{O}_2$  and  $\text{HO}_x$ -radicals are only slightly influenced. The lack of enhancements of these species and the enhancement of  $\text{O}_3$  point towards ozone build-up, and indicate that we most likely probed an aged air mass from an up-wind convective event that had occurred recently (DeCaria et al., 2005).

Signatures of rather fresh convective injection into the UT are found between 13:45 and 13:58 UTC, with enhancements above background concentrations observed for  $\text{CH}_3\text{OH}$ ,  $\text{CH}_3\text{COCH}_3$ ,  $\text{NO}$ ,  $\text{H}_2\text{O}_2$ ,  $\text{CH}_4$  and  $\text{CO}$  and a slight decline of  $\text{O}_3$  mixing ratios, indicating recent transport from lower layers of the troposphere. Formaldehyde does not show clearly enhanced mixing ratios. The strong increase in  $\text{NO}$  indicates production by lightning, which was directly observed in the area (see Fig. 4).

The major convective event associated with the northernmost thunderstorm cell was probed between 14:27 and 14:42 UTC (marked by the red box in Fig. 6). Before entering the outflow, but in close proximity to the convective cell, all trace gases with the exception of  $\text{O}_3$  showed significant decreases in mixing ratios. Between 14:10 and 14:27 UTC,  $\text{CO}$  and  $\text{CH}_4$  dropped to mixing ratios around 65 and 1770 ppbv, respectively, while  $\text{O}_3$  increased to 130 ppbv, indicating downward transport from the stratosphere. Maps of potential vorticity indicate that the local tropopause was about 1–2 km above the aircraft flight track. It has been postulated by Poulida et al. (1996) and later demonstrated by

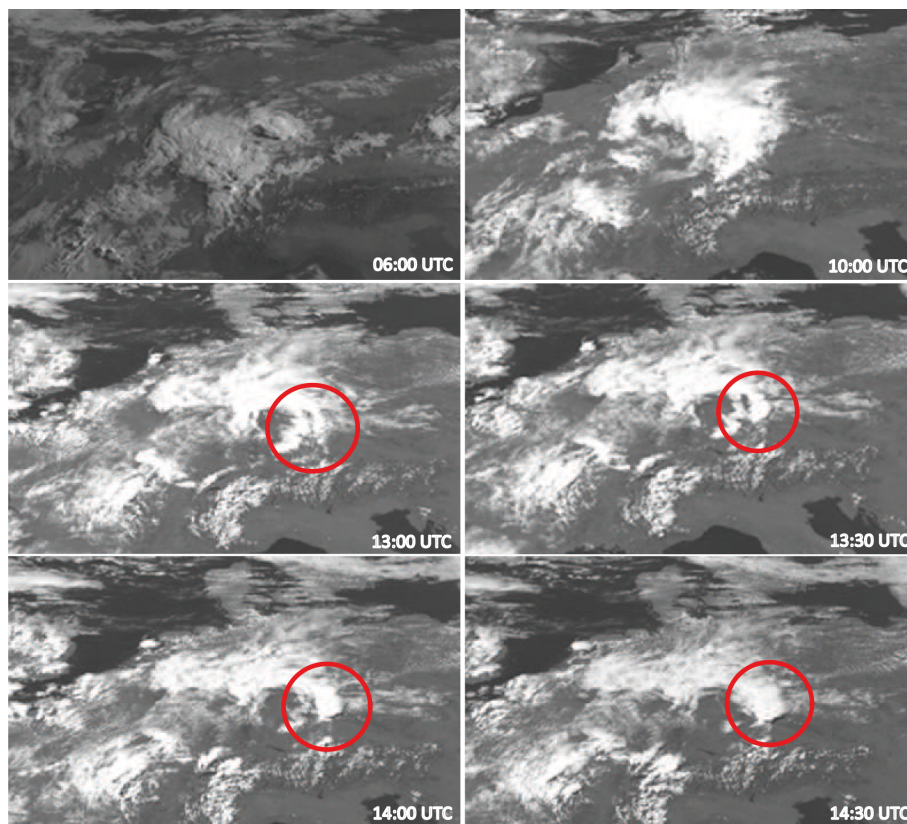


**Figure 3.** Temporal evolution (06:00, 10:00, 13:00, 13:30, 14:00 and 14:30 UTC from top to bottom) of the MCS over Germany observed from Meteosat, obtained from the High-Resolution Visible (HRV) channel.

Pan et al. (2014) that convective cells in the mid-latitudes are often surrounded by  $O_3$  rich air masses associated with transport from the stratosphere, and this phenomenon was also observed during this flight.

As mentioned above, the outflow of the northernmost cell was probed between 14:27 and 14:42 UTC in cloud-free air. Here all trace gases and radicals under investigation show significant changes in mixing ratios. Table 1 lists the changes in mixing ratios in the outflow, the surrounding UT and the enhancement ratio (outflow : surrounding air). The mixing ratios for the surrounding air masses were determined from a part of the flight around 14:15 UTC up-wind of the thunderstorm and before the period affected by the stratospheric influence described above. Values greater than unity for enhancement ratios are reported for all species except  $O_3$ , with a ratio less than 1. These enhancements vary between 4 % for  $CH_4$  and 700 % for  $NO$ , while  $O_3$  in the outflow was 20 % lower than in the surrounding air masses. Even higher enhancement ratios are observed for  $HCHO$ , though also related to the uncertainty in the mixing ratio for the surrounding air mass that was below the detection limit of the instrument. Besides  $HCHO$ , the strongest enhancement is observed for  $NO$ , most probably due to lightning.

After probing the outflow, the aircraft performed a descent into the boundary layer ahead of the thunderstorm over Dresden (marked by the blue box in Fig. 6). Vertical profiles from this part of the flight (between 14:20 and 15:25 UTC) are shown in Fig. 7. Visual inspection of Fig. 7 indicates that mixing ratios for the longer-lived, insoluble trace gases  $CO$ ,  $CH_4$ ,  $CH_3COCH_3$  and  $CH_3OH$  in the outflow are of the same order of magnitude as in the inflow area, i.e. the boundary layer towards the north-east. The mixing ratios of  $NO$ ,  $O_3$  and  $OH$  in the outflow are higher than in the inflow, while for  $HO_2$ ,  $HCHO$  and  $H_2O_2$  we find the reverse. The influence of the high  $NO$  on  $HO_x$  partitioning has been addressed by Regelin et al. (2013) and will not be discussed here. From the behaviour of the longer-lived, insoluble tracers, and assuming that the measurements in the boundary layer are representative of the in-flow of the thunderstorm cell, we infer that the convection transported nearly undiluted boundary-layer air into the UT. Table 2 shows that the median (mean  $\pm 1\sigma$ ) ratios of outflow to inflow mixing ratios for  $CO$ ,  $CH_4$ , methanol and acetone were 0.93 ( $0.94 \pm 0.04$ ), 0.99 ( $0.99 \pm 0.01$ ), 0.93 ( $0.93 \pm 0.10$ ) and 1.22 ( $1.23 \pm 0.12$ ) respectively, and thus not significantly different from unity considering their  $2\sigma$  variability. This indicates that the contribution of entrainment is insignificant for the outflow re-

**Table 1.** Median mixing ratios of different species in the outflow region of the thunderstorm cloud and its surroundings, including the enhancement ratios.

Species	Mixing ratio outflow region (ppbv)	Mixing ratio surrounding (ppbv)	Ratio (outflow region) : (surrounding)
CO	118.5	63.7	1.86
CH <sub>4</sub>	1852.8	1785.6	1.04
HCHO	1.45	0.02	90
O <sub>3</sub>	83.8	104.8	0.80
H <sub>2</sub> O <sub>2</sub>	1.25	0.91	1.37
HO <sub>2</sub> (pptv)	6.63	2.71	2.44
OH (pptv)	3.3	0.73	4.51
NO	0.96	0.12	7.75
Acetone	2.84	0.64	4.44

**Table 2.** Mixing ratios observed in the out- and inflow regions, and their ratios. The median, mean and 1 $\sigma$  standard deviation of all measurements are listed.

Species	Mixing ratio outflow region (ppbv)	Mixing ratio inflow region (ppbv)	Ratio (outflow region) : (inflow region)
CO	118.5 (119.8 $\pm$ 3.9)	127.8 (127.5 $\pm$ 3.0)	0.93 (0.94 $\pm$ 0.04)
CH <sub>4</sub>	1852.8 (1853.1 $\pm$ 12.0)	1876.7 (1876.4 $\pm$ 10.4)	0.99 (0.99 $\pm$ 0.01)
HCHO	1.45 (1.47 $\pm$ 0.11)	2.70 (2.69 $\pm$ 0.42)	0.54 (0.55 $\pm$ 0.09)
H <sub>2</sub> O <sub>2</sub>	1.25 (1.28 $\pm$ 0.09)	2.11 (2.09 $\pm$ 0.21)	0.59 (0.61 $\pm$ 0.08)
O <sub>3</sub>	83.8 (83.5 $\pm$ 2.6)	80.8 (81.2 $\pm$ 2.7)	1.04 (1.03 $\pm$ 0.05)
NO	0.96 (0.99 $\pm$ 0.20)	0.05 (0.05 $\pm$ 0.03)	19.2 (19.8 $\pm$ 12.54)
OH (pptv)	3.3 (2.91 $\pm$ 0.93)	0.28 (0.26 $\pm$ 0.13)	11.79 (11.19 $\pm$ 6.64)
HO <sub>2</sub> (pptv)	6.63 (6.04 $\pm$ 1.04)	16.94 (18.41 $\pm$ 3.08)	0.39 (0.33 $\pm$ 0.08)
Acetone	2.84 (2.82 $\pm$ 0.21)	2.33 (2.30 $\pm$ 0.22)	1.22 (1.23 $\pm$ 0.12)
Methanol	7.19 (7.12 $\pm$ 0.36)	7.71 (7.63 $\pm$ 0.64)	0.93 (0.93 $\pm$ 0.10)

gion, in line with previous observations. Hauf et al. (1995) concluded from a case study of a thunderstorm over Basel (Switzerland) that the cloud contained “protective cores”, in which air from the boundary layer was transported almost undiluted to the anvil. Similar observations were reported by Poulida et al. (1996) and Ström et al. (1999). Thus, the lower than unity values for outflow : inflow ratios for HCHO and H<sub>2</sub>O<sub>2</sub> of 0.54 (0.55  $\pm$  0.09) and 0.59 (0.61  $\pm$  0.08), respectively, are most likely due to partial rain-out of these soluble species. Other studies (Bertram et al., 2007; Fried et al., 2016) derived much lower ratios between outflow and boundary layer inflow, indicating significant entrainment. To estimate the potential role of entrainment for our measurements we apply a two-box model (Cohan et al., 1999) to calculate outflow (OF) mixing ratios from the inflow (IN) and the entrainment (EN) according to  $OF = xEN + (1 - x)IN$ .

Using values for OF, IN and EN from Tables 1 and 2 and Fig. 7 we derive the following entrainment rates: 24 % (CO), 26 % (CH<sub>4</sub>), 30 % (Acetone) and 19 % (methanol) indicating that roughly 75 % of the air in the outflow stems from the boundary layer. Thus assuming an average value of 25 % for the entrainment rate we calculate maximum mixing ratios for

HCHO and H<sub>2</sub>O<sub>2</sub> at the storm core of 2.05 and 1.82 ppbv, respectively.

As illustrated in the schematic in Fig. 8, the 5 min measurements in the outflow were made in clear, cloud-free air at a distance between 50 and 150 km from the anvil. At a wind speed of 30 m s<sup>-1</sup> this would correspond to a transport time of 30 to 90 min, which is sufficient for secondary photochemistry (production or destruction) to become a significant contributor to the budgets of shorter-lived species like HCHO and H<sub>2</sub>O<sub>2</sub>. For example, Bozem et al. (2017) calculated the potential net ozone production rate from in situ observation in this convective event and derived a rate of 1.9  $\pm$  0.28 ppbv h<sup>-1</sup>, indicating secondary ozone formation of 1–3 ppbv in the outflow, explaining the slight difference in O<sub>3</sub> between the inflow (80.8 ppbv; 81.2  $\pm$  2.7 ppbv) and outflow region (83.8 ppbv; 83.5  $\pm$  2.6 ppbv) (Table 2).

As shown by Fried et al. (2008), the temporal evolution of the HCHO mixing ratio depends on the concentration of HCHO at the cloud top, the concentrations of HCHO precursors and radicals, and the processing time. Within the first few hours it is unlikely that the HCHO concentration will reach steady state. Here we will use a box model to simulate the temporal evolution of HCHO and H<sub>2</sub>O<sub>2</sub> mixing ratios in

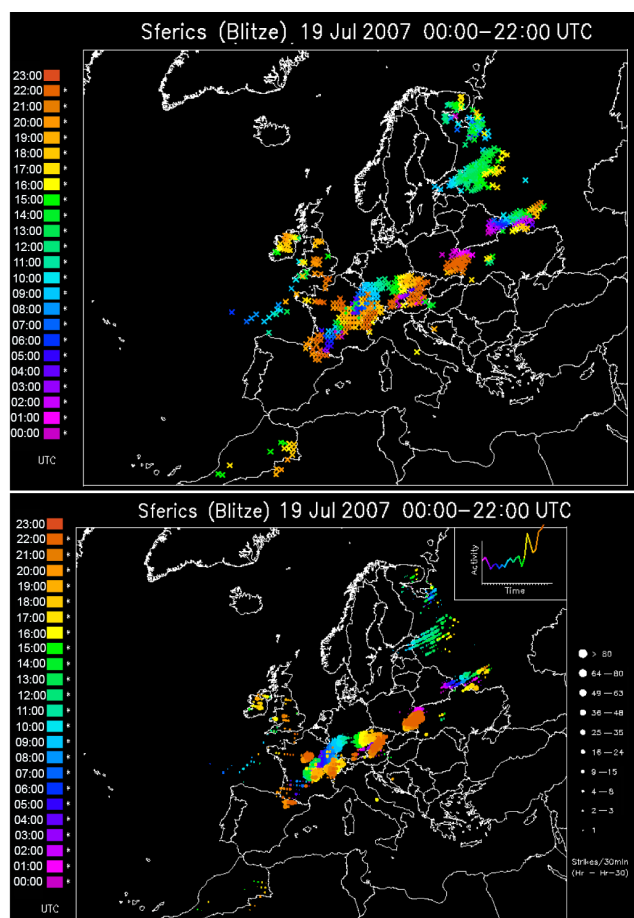


**Figure 4.** (top panel) Lightning activity from 00:00 to 22:00 UTC on 19 July 2007 over Europe. (bottom panel) Lightning flash occurrence in flashes per 30 min for the same time interval. The colour code indicates the time of flash detection. Source: [www.wetterzentrale.de](http://www.wetterzentrale.de)

the outflow region after exiting the cloud. Please note that this model study neglects mixing with background air. This is justified by the ratios between inflow and outflow given in Table 2 for the longer-lived species, which are close to unity, indicating insignificant mixing with surrounding air masses.

### 3.3 Temporal evolution of HCHO and H<sub>2</sub>O<sub>2</sub> mixing ratios

To calculate the temporal evolution of HCHO and H<sub>2</sub>O<sub>2</sub> with the MECCA model, we constrained it with measured median OH, HO<sub>2</sub>, CO, CH<sub>4</sub>, CH<sub>3</sub>OH, CH<sub>3</sub>COCH<sub>3</sub>, O<sub>3</sub> and NO mixing ratios, and photolysis rates derived from the radiation transfer model TUV (<https://www2.acom.ucar.edu/modeling/tropospheric-ultraviolet-and-visible-tuv-radiation-model>; Madronich and Flocke, 1999), based on observed  $j(\text{NO}_2)$  frequencies. Calculations of chemical production and loss were performed for 2 hours with a time step of 15 min. In

general, the model runs indicate a strong dependency of the mixing ratio evolution on processing time and the amount of HCHO and H<sub>2</sub>O<sub>2</sub> leaving the convective cloud (initial values). At high HCHO and H<sub>2</sub>O<sub>2</sub> initial concentrations, photochemical destruction due to photolysis and reaction with OH prevails (the loss terms are proportional to the initial concentration), while at low initial concentrations secondary production from precursors dominate. Therefore, a number of sensitivity studies were performed that take into account the uncertainties in initial values and processing time. To account for variations in the input parameters and uncertainties of the rate constants of the model we performed additional sensitivity calculations based on the Monte Carlo method, by varying initial concentrations within the  $1\sigma$  uncertainties and rate constants by up to  $\pm 80\%$ .

Figure 9 shows the temporal evolution of HCHO mixing ratios in the outflow as simulated with MECCA. The blue area (median with standard deviation) indicates the observed HCHO concentration in the outflow ( $1.45 \pm 0.11$  ppbv). Sensitivity studies were performed with different initial HCHO concentrations. A first run was performed with an initial HCHO mixing ratio of 0.02 ppbv, corresponding to background conditions (Table 1). This case study represents near-complete removal of HCHO during convective uplifting due to cloud processing, followed by subsequent secondary production from HCHO precursors in the cloud-free outflow. Note that all precursors and radical levels are initialized at observed values in the outflow and do not change during the processing. The red curve in Fig. 9 starts at background HCHO mixing ratios, and exhibits significant production of HCHO during the first 60 min with a rate of approximately  $0.01 \text{ ppbv min}^{-1}$  with a maximum HCHO mixing ratio of 0.56 ppbv (range 0.51–0.61 ppbv), corresponding to the minimum and the maximum of the Monte Carlo simulation after around 90 min, and slowly decreasing values afterwards. These results compare well to box model studies of secondary HCHO formation after convective events reported by Stickler et al. (2006) and Fried et al. (2008). Since the mixing ratios in this simulation are at any time smaller than values observed in the outflow, we can assume that a significant portion of HCHO observed in the outflow is due to vertical transport from the inflow region.

A second run (not shown) was performed with an initial HCHO mixing ratio corresponding to the observed value in the outflow ( $1.45 \pm 0.11$  ppbv). Photochemical loss of HCHO through photolysis and reaction with OH dominates the temporal evolution of formaldehyde in this run, with loss rates of up to  $0.02 \text{ ppbv min}^{-1}$ . This case study demonstrates that HCHO initial values have to be larger than observed mixing ratios in the outflow if we take photochemical processing into account. On the other hand, if we fully neglect photochemical processing by setting the processing time to zero, the observed concentration in the outflow is identical to the amount transported upwards in the convective cloud, providing a lower limit for the cloud top outflow. In a third sen-

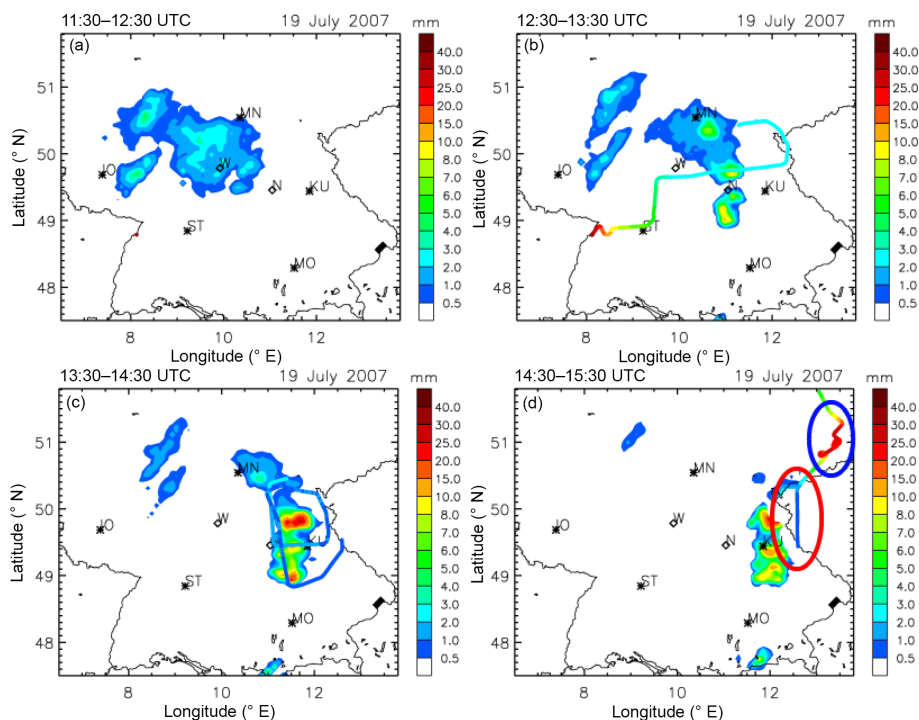


**Figure 5.** (a–d): RADOLAN data of the German weather service. Precipitation intensity is colour coded in millimetres per hour. The flight tracks are also shown (red: low flight levels, blue: high flight levels). The red marked area in the lower panel shows the outflow region, the blue one the inflow region in the boundary layer nearby Dresden. Data were provided by M. Zimmer with permission of E. Weigel (German weather service).

sitivity study we assumed undiluted transport of HCHO from the boundary layer to the cloud top. Starting with an initial value of  $2.70 \pm 0.42$  ppbv corresponding to the HCHO mixing ratio in the inflow, the green curve in Fig. 9 shows strong photochemical loss of HCHO throughout the simulation. The envelope given by the minimum and maximum of the initial concentrations and the Monte Carlo simulation intercepts the observed HCHO mixing ratio range between 20 and 52 min (vertical dashed lines). Due to both the uncertainty of the HCHO initial values and the elapsed processing time it is not possible to assign a single value to the HCHO mixing ratio in the cloud outflow. Instead we used a range corresponding to a minimum value given by the measured HCHO mixing ratio in the cloud-free outflow ( $1.45 \pm 0.11$  ppbv) and assuming zero processing, and a maximum value assuming undiluted HCHO transport from the inflow region ( $2.70 \pm 0.42$  ppbv) and a processing time of 20 to 52 min. To study the role of entrainment a final sensitivity run (black dashed line) was performed with a mixing ratio for HCHO at the storm core of 2.05 ppbv, calculated based on an entrainment rate of 25%. This curve is only slightly below the green curve and yields slightly lower processing times.

Figure 10 shows the temporal evolution of  $\text{H}_2\text{O}_2$  in the outflow region calculated with MECCA. Independent of the initial  $\text{H}_2\text{O}_2$  mixing ratio all simulations indicate a photochemical loss of hydrogen peroxide in the first 2 h after con-

vective injection. Assuming a processing time between 20 and 52 min deduced from the HCHO study (vertical dashed lines), the best fit for the initial  $\text{H}_2\text{O}_2$  concentration is obtained for a range between 1.42 and 1.45 ppbv (brown trace in Fig. 10). Lower initial values (red trace for background conditions corresponding to zero transport) or higher values (green trace for complete transport from the inflow region to the outflow and the black dashed line for an assumed entrainment rate of 25%) are at no time compatible with the observations (blue bar). As in the case of HCHO we will again provide a range of  $\text{H}_2\text{O}_2$  initial values that are compatible with the observations in the outflow, with a minimum of  $1.25 \pm 0.09$  ppbv given by the observed mixing ratio and no photochemical processing and a maximum of  $1.435 \pm 0.015$  ppbv provided for the model best fit at processing times between 20 and 52 min. It should be mentioned that the MECCA simulations are based on gas-phase chemistry only. Hydrogen peroxide formation in the liquid phase by  $\text{HO}_2$  or  $\text{O}_3$  dissolution is ignored. Based on short transport times from the boundary layer to the UT of the order of 30 min at vertical velocities of  $5 \text{ m s}^{-1}$  and a depth of 9 km, the  $\text{H}_2\text{O}_2$  production by these processes is negligible (Prather and Jacob, 1997; Jacob, 2000).

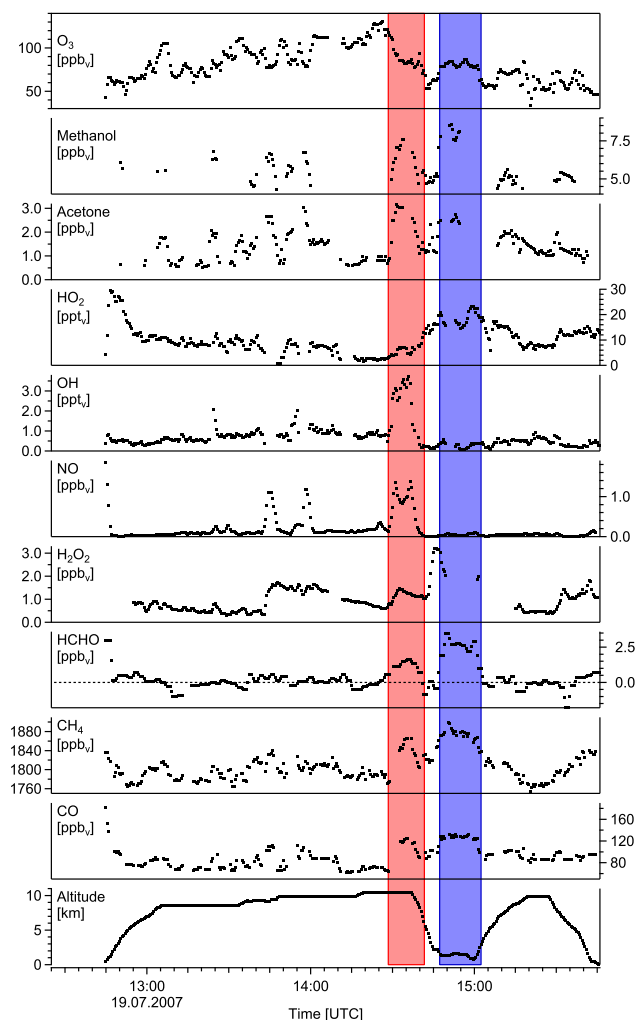


**Figure 6.** Time series of parameters measured on 19 July 2007. The red area marks the outflow region, the blue area the inflow region.

### 3.4 Estimation of scavenging efficiencies for HCHO and H<sub>2</sub>O<sub>2</sub>

Based on the model results presented above, we estimate the HCHO mixing ratio at the cloud top exit to be in the range between 1.45 and 2.70 ppbv. This corresponds to the amount of HCHO transported from the inflow region to the top of the cloud. Assuming no chemical processing in the cloud, the ratio between the modelled cloud top mixing ratio and the mixing ratio in the inflow region yields the transport efficiency for HCHO at a range of 53–100%. This indicates a strong contribution of transport to the HCHO budget in the outflow, which corresponds to minor cloud scavenging, i.e. at an efficiency between 0 and 47% (amount of HCHO lost within the cloud). For H<sub>2</sub>O<sub>2</sub> a similar analysis yields a cloud top mixing ratio of 1.25 to 1.45 ppbv, a transport efficiency of 59 to 68% and a corresponding scavenging efficiency of 32 to 41%.

## 4 Discussion and conclusions

The main result of this study is that HCHO and H<sub>2</sub>O<sub>2</sub> observed in the outflow of a deep convective cloud in the UT are largely controlled by transport from the lower troposphere. Post-convective photochemical processing in cloud-free air cannot explain the observations of both species since chemical loss processes are found to dominate. This means that at least 53% of HCHO and at least 59% of H<sub>2</sub>O<sub>2</sub> from the boundary layer reach the cloud top. These percentages increase further if we take into account photochemical processing during a time period of 20 to 52 min, yielding 100% (HCHO) and 68% (H<sub>2</sub>O<sub>2</sub>), respectively. This is a consequence of the dominance of loss processes after injection into the outflow region. Formaldehyde is more sensitive to the post-cloud processing due to its shorter photochemical lifetime, resulting in a larger range of potential initial values that are compatible with the observations. From these results we deduced scavenging efficiencies for HCHO and H<sub>2</sub>O<sub>2</sub> of 0 to 47% and 32–41%, respectively.

Several studies reported in the literature show that HCHO in the UT convective outflow can be significantly enhanced. Previous observation-based studies have attributed this HCHO enhancement either completely (Stickler et al., 2006; Fried et al., 2008a) or largely (60%, Borbon et al., 2012) to secondary photochemical production in the outflow. The studies of Stickler et al. (2006) and Fried et al. (2008) involved substantial distance from the convective outflow, and represented extensive processing of air within the UT. This might explain the high contributions for secondary production found in these studies, while we simulate strong photochemical loss of HCHO in the first 2 hours after convective injection. Studies by Marie et al. (2000), Barth et al. (2001) and Marie et al. (2003) were based on model simulations and observations, and addressed the influence of convective transport on the budget of HCHO in the UT. They emphasized the importance of HCHO scavenging and discussed the effect of incomplete retention by hydrometeors during freezing. Barth et al. (2007) considered gas, liquid and frozen water chemistry, and estimated scavenging efficiencies for HCHO of 46–67%. This is higher than the range presented here, which agrees better with the findings of Borbon et al. (2012), who derived a very small scavenging efficiency of  $4 \pm 1\%$  for a MSC storm over a tropical forest region of Oueme and values of  $26 \pm 8$ ,  $39 \pm 12$  and  $13 \pm 4\%$  for three storms over other regions of west Africa. Analysing data from a number of storms over North America as part of the DC3 aircraft campaign, Fried et al. (2016) derived scavenging efficiencies of  $54 \pm 3$ ,  $54 \pm 6$ ,  $58 \pm 13$  and  $41 \pm 4\%$  for four storms in May and June 2012, which is again higher than our result (range 0–47%).

The scavenging efficiency for H<sub>2</sub>O<sub>2</sub> of 32–41% deduced in this study is lower than most values reported in the literature thus far. Based on 3-D-model results Barth et al. (2007) report a range between 55 and 65%. From in situ observa-

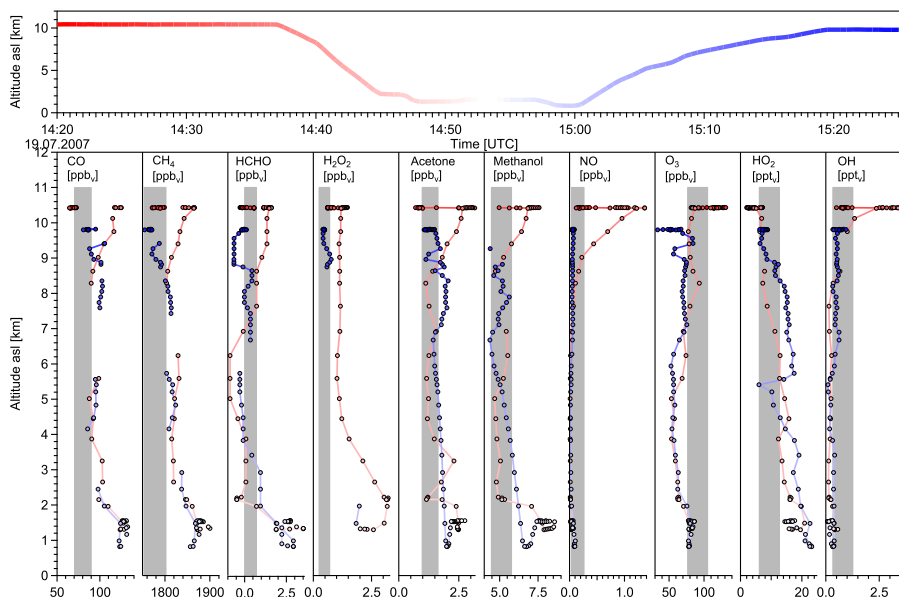


**Figure 7.** Vertical profiles from in situ measurements on 19 July 2007. Colour coding indicates altitude (see upper panel). The grey shaded area shows typical mixing ratios in the upper troposphere.

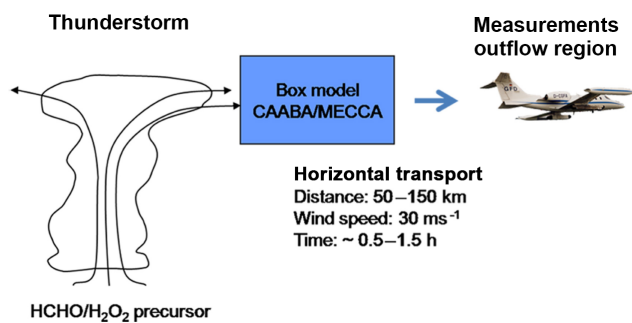


**Figure 8.** Scheme for the initialisation of the chemical box model studies.

tions in DC3,  $\text{H}_2\text{O}_2$  scavenging efficiencies between 79 and 97 % were deduced (Barth et al., 2016, Bela et al., 2016). As has been shown by a number of model studies (Marie et al., 2000, 2003; Barth et al., 2001; Bela et al., 2016) the  $\text{H}_2\text{O}_2$  scavenging efficiency strongly depends on the fate of  $\text{H}_2\text{O}_2$  during freezing of cloud particles. Incomplete retention can lead to degassing of  $\text{H}_2\text{O}_2$  from the droplets and reduce scavenging efficiencies. The retention coefficient describing the fraction of a dissolved species retained in the droplet during freezing is highly uncertain. Reported values in the literature for  $\text{H}_2\text{O}_2$  retention vary between 5 and 100 % (Iribarne and Pyshnov, 1990; Snider et al., 1992; Conklin et al., 1993; Snider and Huang, 1998). Experiments in the Mainz vertical wind tunnel lab yielded a  $\text{H}_2\text{O}_2$  retention coefficient of  $52 \pm 8$  % (von Blohn et al., 2011), which is about 10 to 20 % higher than our results. It should be mentioned that such an analysis will also depend on the ice fraction in the clouds that

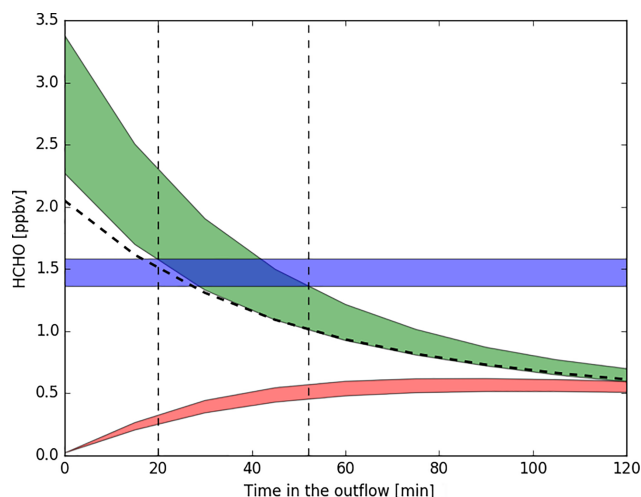


**Figure 9.** Simulated temporal evolution of HCHO mixing ratios in the outflow region. Coloured bars show the variance from sensitivity studies with randomly-varied rate constants and concentrations. The blue bar indicates the range of observed values in the outflow. The red curve simulates photochemical production assuming zero transport from the inflow area, while the green curve shows photochemical degradation assuming 100 % transport from the inflow area. The dashed line is a sensitivity study assuming an entrainment rate of 25 %. The dashed vertical lines indicate the best fits for the processing time.

are typically mixed-phase systems. Ice fractions are expected to vary so that retention coefficients may fluctuate accordingly.

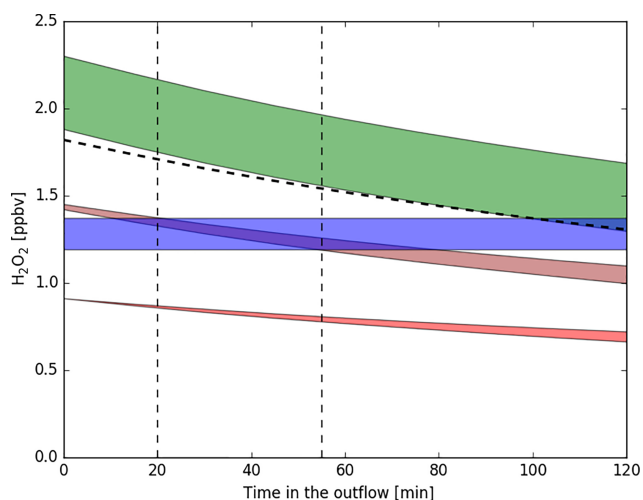


**Figure 10.** Simulated temporal evolution of  $\text{H}_2\text{O}_2$  mixing ratios in the outflow region. Coloured bars show the variance from sensitivity studies with randomly-varied rate constants and concentrations. The blue bar indicates the range of observed values in the outflow. The red curve simulates photochemical change assuming zero transport from the inflow area, while the green curve shows photochemical degradation assuming 100 % transport from the inflow area. The dashed line is a sensitivity study assuming an entrainment rate of 25 %. The brown curve is the best fit for processing times deduced from the HCHO study (dashed vertical lines).

Overall our results compare well to literature values, with scavenging efficiencies for both HCHO and  $\text{H}_2\text{O}_2$  being at the lower end of those reported. The model calculations in Sect. 3.3 indicate that the temporal evolution of both HCHO and  $\text{H}_2\text{O}_2$  after convective injection depends strongly on the initial values and the processing time. In particular during the first 120 min, when both species are far off from photo-stationary state, changes are very large and give rise to large uncertainties. Fried et al. (2016) also pointed out that the definition of inflow and outflow regimes can be critical. They report a case of weak convection, and their analysis provided a rather high scavenging efficiency for HCHO of  $81 \pm 5\%$ , attributed to a mismatch between in- and outflow of the system. Establishing a connection between the timing and location of the inflow area and the corresponding outflow of a convective system is the most critical aspect of this type of study, since Lagrangian experiments are practically not possible. One way to establish an unambiguous connection between in- and outflow would be through the use of an artificial tracer released in the inflow area (Ren et al., 2015), ideally from a second airplane. Here we have to rely on sequential measurement, first in the outflow and later in the potential inflow area. Due to the time shift associated with the vertical transport and the movement of the convective system itself it is not possible to unambiguously determine the inflow area. The inflow area may be considered representative if trace gases are distributed homogeneously with

respect to space and time. The fact that several conservative tracers show similar ratios between in- and outflow is an indication that this assumption is fulfilled. Additionally, Fig. 6 of Klippel et al. (2011) indicates that HCHO and  $\text{H}_2\text{O}_2$  mixing ratios in the boundary layer are within the range of observations made during all HOOVER II flights in the latitude belt from  $50$  to  $57.5^\circ$  N. It is not possible to determine the height of the layer from which the inflow takes place. While CO and some other tracers can be assumed to be well mixed in the boundary layer, this is not the case for  $\text{H}_2\text{O}_2$  and to a lesser extend also for HCHO, which exhibit strong gradients in the lower troposphere (e.g. Klippel et al., 2011).

Our results partly contradict the analysis of DC3 measurements (Fried et al., 2016; Bela et al., 2016; Barth et al., 2016) that yielded much higher scavenging efficiencies. If we assume an average scavenging efficiency of 50 % for HCHO, as reported by Fried et al. (2016), the measured HCHO mixing ratio of 1.45 ppbv in the outflow corresponds to a minimum inflow mixing ratio of 3 ppbv, neglecting entrainment and photochemical processing in the outflow area. The same calculation for  $\text{H}_2\text{O}_2$  assuming a scavenging efficiency of 80 % (Barth et al., 2016) and an outflow mixing ratio of 1.25 ppbv, would yield an  $\text{H}_2\text{O}_2$  mixing ratio in the inflow area of  $\sim 9$  ppbv. Based on the observations of both species during HOOVER II (Klippel et al., 2011) the simultaneous occurrence of these mixing ratios for both species, in particular at the same altitude, is very unlikely. Thus, applying the scavenging efficiencies derived from the DC3 campaign would yield inconsistent results. Unfortunately, differences in the storm dynamics and microphysics between DC3 and HOOVER cannot be investigated since these details are not available for HOOVER. Differences to DC3 might be due to degassing from evaporating hydrometeors since the HOOVER measurements were performed in cloud-free air at considerable distance from the convective core, while the DC3 observations were made in the anvil (Fried et al., 2016; Bela et al., 2016; Barth et al., 2016).

*Data availability.* Readers who are interested in the data should contact the authors: Heiko Bozem (bozemh@uni-mainz.de) or Horst Fischer (horst.fischer@mpic.de).

*Competing interests.* The authors declare that they have no conflict of interest.

*Acknowledgements.* The authors would like to acknowledge the support from the HOOVER team, enviscope GmbH (Frankfurt) and GFD (Gesellschaft für Zielflugdarstellung, Hohn).

The article processing charges for this open-access publication were covered by the Max Planck Society.

Edited by: Timothy Bertram

Reviewed by: three anonymous referees

## References

- Barth, M. C., Stuart, A. L., and Skamarock, W. C.: Numerical simulations of the July 10, 1996, Stratospheric-Tropospheric Experiment: Radiation, Aerosols, and Ozone (STERAO)-Deep Convection experiment storm: Redistribution of soluble tracers, *J. Geophys. Res.*, 106, 12381–12400, <https://doi.org/10.1029/2001JD900139>, 2001.
- Barth, M. C., Kim, S.-W., Skamarock, W. C., Stuart, A. L., Pickering, K. E., and Ott, L. E.: Simulations of the redistribution of formaldehyde, formic acid, and peroxides in the 10 July 1996 Stratospheric-Tropospheric Experiment: Radiation, Aerosols, and Ozone deep convection storm, *J. Geophys. Res.*, 112, D13310, <https://doi.org/10.1029/2006JD008046>, 2007.
- Barth, M. C., Cantrell, C. A., Brune, W. H., Rutledge, S. A., Crawford, J. H., Huntrieser, H., Carey, L. D., MacGorman, D., Weisman, M., Pickering, K. E., Bruning, E., Anderson, B., Apel, E., Biggerstaff, M., Campos, T., Campuzano-Jost, P., Cohen, R., Crouse, J., Day, D. A., Diskin, G., Flocke, F., Fried, A., Garland, C., Heikes, B., Honomichl, S., Hornbrook, R., Huey, L. G., Jimenez, J. L., Lang, T., Lichtenstern, M., Mikoviny, T., Nault, B., O'Sullivan, D., Pan, L. L., Peischl, J., Pollack, I., Richter, D., Riemer, D., Ryerson, T., Schlager, H., Clair, J. St., Walega, J., Weibring, P., Weinheimer, A., Wennberg, P., Wisthaler, A., Wooldridge, P. J., and Ziegler, C.: The Deep Convective Clouds and Chemistry (DC3) Field Campaign, *Bull. Am. Meteor. Soc.*, 96, 1281–1309, <https://doi.org/10.1175/BAMS-D-13-00290.1>, 2015.
- Barth, M. C., Bela, M. M., Fried, A., Wennberg, P. O., Crouse, J. D., Clair, J. M. St., Blake, N. J., Blake, D. R., Homeyer, C. R., Brune, W. H., Zhang, L., Mao, J., Ren, X., Ryerson, T. B., Pollack, I. B., Peischl, J., Cohen, R. C., Nault, B. A., Huey, L. G., Liu, X., and Cantrell C. A.: Convective transport and scavenging of peroxides by thunderstorms observed over the central U.S. during DC3, *J. Geophys. Res.-Atmos.*, 121, 4272–4295, <https://doi.org/10.1002/2015JD024570>, 2016.
- Bela, M. M., Barth, M. C., Toon, O. B., Fried, A., Homeyer, C. R., Morrison, H., Cummings, K. A., Li, Y., Pickering, K. E., Allen, D. J., Yang, Q., Wennberg, P. O., Crouse, J. D., St. Clair, J. M., Teng, A. P., O'Sullivan, D., Huey, L. G., Chen, D., Liu, X., Blake, D. R., Blake, N. J., Apel, E. C., Hornbrook, R. S., Flocke, F., Campos, T., and Diskin, G.: Wet scavenging of soluble gases in DC3 deep convective storms using WRF-Chem simulations and aircraft observations, *J. Geophys. Res.-Atmos.*, 121, 4233–4257, <https://doi.org/10.1002/2015JD024623>, 2016.
- Bertram, T. H., Perring, A. E., Wooldridge, P. J., Crouse, J. D., Kwan, A. J., Wennberg, P. O., Scheuer, E., Dibb, J., Avery, M., Sachse, G., Vay, S. A., Crawford, J. H., McNaughton, C. S., Clarke, A., Pickering, K. E., Fuelberg, H., Huey, G., Blake, D. R., Singh, H. B., Hall, S. R., Shetter, R., Alan Fried, Heikes, B. G., and Cohen, R. C.: Direct measurements of the convective recycling of the upper troposphere. *Science*, 315, 816–820, <https://doi.org/10.1126/science.1134548>, 2007.
- Borbon, A., Ruiz, M., Bechara, J., Aumont, B., Chong, M., Huntrieser, H., Marie, C., Reeves, C. E., Scialom, G., Hamburger, T., Stark, H., Afif, C., Jambert, C. Mills, G., Schlager, H., and Perros, P. E.: Transport and chemistry of formaldehyde by mesoscale convective systems in West Africa during AMMA 2006, *J. Geophys. Res.*, 117, D12301, <https://doi.org/10.1029/2011JD017121>, 2012.
- Bozem, H., Butler, T. M., Lawrence, M. G., Harder, H., Martinez, M., Kubistin, D., Lelieveld, J., and Fischer, H.: Chemical processes related to net ozone tendencies in the free troposphere, *Atmos. Chem. Phys.*, 17, 10565–10582, <https://doi.org/10.5194/acp-17-10565-2017>, 2017.
- Chatfield, R. B. and Crutzen, P. J.: Sulfur dioxide in remote oceanic air: Cloud transport of reactive precursors, *J. Geophys. Res.*, 89, 7111–7132, <https://doi.org/10.1029/JD089iD05p07111>, 1984.
- Cohan, D. S., Schultz, M. G., Jacob, D. J., Heikes, B. G., and Blake, D. R.: Convective injection and photochemical decay of peroxides in the tropical upper troposphere: Methyl iodide as a tracer of Mariene convection, *J. Geophys. Res.*, 104, 5717–5724, <https://doi.org/10.1029/98JD01963>, 1999.
- Colomb, A., Williams, J., Crowley, J., Gros, V., Hofmann, R., Salisbury, G., Kluepfel, T., Kormann, R., Stickler, A., Forster, C., and Lelieveld, J.: Airborne measurements of trace organic species in the upper troposphere over Europe: the impact of deep convection, *Environ. Chem.*, 3, 244–259, <https://doi.org/10.1071/EN06020>, 2006.
- Conklin, M. H., Sigg, A., Neftel, A., and Bales, R. C.: Atmosphere-snow transfer function for H<sub>2</sub>O<sub>2</sub>: Microphysical considerations, *J. Geophys. Res.*, 98, 18367–18376, <https://doi.org/10.1029/93JD01194>, 1993.
- Crutzen, P. J. and Lawrence, M. G.: The impact of precipitation scavenging on the transport of trace gases: A 3-dimensional model sensitivity study, *J. Atmos. Chem.*, 37, 81–112, <https://doi.org/10.1023/A:1006322926426>, 2000.
- DeCaria, A. J., Pickering, K. E., Stenchikov, G. L., and Ott, L. E.: Lightning-generated NO<sub>x</sub> and its impact on tropospheric ozone production: A three-dimensional modeling study of a Stratosphere-Troposphere Experiment: Radiation, Aerosols and Ozone (STERAO-A) thunderstorm, *J. Geophys. Res.*, 110, D14303, <https://doi.org/10.1029/2004JD005556>, 2005.
- Dickerson, R. R., Huffman, G. J., Luke, W. T., Nunnermacker, L. J., Pickering, K. E., Leslie, A. C. D., Lindsey, C. G., Slinn, W. G. N., Kelly, T. J., Daum, P. H., Delany, P. H., Greenberg, J. P., Zimmerman, P. R., Boatman, J. F., Ray, J. D., and Stedman, D. H.: Thunderstorms – An important mechanism in the transport of air pollutants, *Science*, 235, 460–464, <https://doi.org/10.1126/science.235.4787.460>, 1987.
- Fried, A., Olson, J. R., Walega, J. G., Crawford, J. H., Chen, G., Weibring, P., Richter, D., Roller, C., Tittel, F., Porter, M., Fuelberg, H., Halland, J., Bertram, T. H., Cohen, R. C., Pickering, K. E., Heikes, B. G., Snow, J. A., Shen, H., O'Sullivan, D. W., Brune, W. H., Ren, X., Blake, D. R., Blake, N., Sachse, G., Diskin, G. S., Podolske, J., Vay, S. A., Shetter, R. E., Hall, S. R., Anderson, B. E., Thornhill, L., Clarke, A. D., McNaughton, C. S., Singh, H. B., Avery, M. A., Huey, G., Kim, S., and Millet, D. B.: Role of convection in redistributing formaldehyde to the upper troposphere over North America and the North Atlantic dur-

- ing the summer 2004 INTEX campaign, *J. Geophys. Res.*, 113, D17306, <https://doi.org/10.1029/2007JD009760>, 2008.
- Fried, A., Barth, M. C., Bela, M., Weibring, P., Richter, D., Walega, J., Li, Y., Pickering, K., Apel, E., Hornbrook, R., Hills, A., Riemer, D. D., Blake, N., Blake, D. R., Schroeder, J. R., Luo, Z. J., Crawford, J. H., Olson, J., Rutledge, S., Betten, D., Biggerstaff, M. I., Diskin, G. S., Sachse, G., Campos, T., Flocke, F., Weinheimer, A., Cantrell, C., Pollack, I., Peischl, J., Froyd, K., Wisthaler, A., Mikoviny, T., and Woods, S.: Convective transport of formaldehyde to the upper troposphere and lower stratosphere and associated scavenging in thunderstorms over the central United States during the 2012DC3 study, *J. Geophys. Res.-Atmos.*, 121, 7430–7460, <https://doi.org/10.1002/2015JD024477>, 2016.
- Garstang, M., Scala, J., Greco, S., Harriss, R., Beck, S., Browell, E., Sachse, G., Gregory, G., Hill, G., Simpson, J., Tao, W.-K., and Torres, A.: Trace gas exchanges and convective transports over the Amazonian rain forest, *J. Geophys. Res.*, 93, 1528–1550, <https://doi.org/10.1029/JD093iD02p01528>, 1988.
- Gidel, L. T.: Cumulus cloud transport of transient tracers, *J. Geophys. Res.*, 88, 6587–6599, <https://doi.org/10.1029/JC088iC11p06587>, 1983.
- Gurk, Ch., Fischer, H., Hoor, P., Lawrence, M. G., Lelieveld, J., and Wernli, H.: Airborne in-situ measurements of vertical, seasonal and latitudinal distributions of carbon dioxide over Europe, *Atmos. Chem. Phys.*, 8, 6395–6403, <https://doi.org/10.5194/acp-8-6395-2008>, 2008.
- Hauf, T., Schulte, P., Alheit, R., and Schlager, H.: Rapid vertical trace gas transport by an isolated midlatitude thunderstorm, *J. Geophys. Res.*, 100, 22957–22970, <https://doi.org/10.1029/95JD02324>, 1995.
- Hosaynali Beygi, Z., Fischer, H., Harder, H. D., Martinez, M., Sander, R., Williams, J., Brookes, D. M., Monks, P. S., and Lelieveld, J.: Oxidation photochemistry in the Southern Atlantic boundary layer: unexpected deviations of photochemical steady state, *Atmos. Chem. Phys.*, 11, 8497–8513, <https://doi.org/10.5194/acp-11-8497-2011>, 2011.
- Iribarne, J. V. and Psychov, T.: The effect of freezing on the composition of supercooled droplets, 1. Retention of HCl, HNO<sub>3</sub>, NH<sub>3</sub> and H<sub>2</sub>O<sub>2</sub>, *Atmos. Environ.*, 24, 383–387, [https://doi.org/10.1016/0960-1686\(90\)90118-7](https://doi.org/10.1016/0960-1686(90)90118-7), 1990.
- Jacob, D. J.: Heterogeneous chemistry and tropospheric ozone, *Atmos. Environ.*, 34, 2131–2159, [https://doi.org/10.1016/S1352-2310\(99\)00462-8](https://doi.org/10.1016/S1352-2310(99)00462-8), 2000.
- Jaeglé, L., Jacob, D. J., Wennberg, P. O., Spivakovsky, C. M., Hanisco, T. F., Lanzendorf, E. J., Hints, E. J., Fahey, D. W., Keim, E. R., Proffitt, M. H., Atlas, E. L., Flocke, F., Schauffler, S., McElroy, C. T., Midwinter, C., Pfister, L., and Wilson, J. C.: Observed OH and HO<sub>2</sub> in the upper troposphere suggest a major source from convective injection of peroxides, *Geophys. Res. Lett.*, 24, 3181–3184, <https://doi.org/10.1029/97GL03004>, 1997.
- Jaeglé, L.: Pumping up surface air, *Science*, 315, 772–773, <https://doi.org/10.1126/science.1138988>, 2007.
- Jenkin, M. E., Saunders, S. M., and Pilling, M. J.: The tropospheric degradation of volatile organic compounds: A protocol for mechanism development, *Atmos. Environ.*, 31, 81–104, [https://doi.org/10.1016/S1352-2310\(96\)00105-7](https://doi.org/10.1016/S1352-2310(96)00105-7), 1997.
- Jöckel, P., Tost, H., Pozzer, A., Brühl, C., Buchholz, J., Ganzeveld, L., Hoor, P., Kerkweg, A., Lawrence, M. G., Sander, R., Steil, B., Stiller, G., Tanarhte, M., Taraborrelli, D., van Aardenne, J., and Lelieveld, J.: The atmospheric chemistry general circulation model ECHAM5/MESSy1: consistent simulation of ozone from the surface to the mesosphere, *Atmos. Chem. Phys.*, 6, 5067–5104, <https://doi.org/10.5194/acp-6-5067-2006>, 2006.
- Jonquière, I. and Marenco, A.: Redistribution by deep convection and long-range transport of CO and CH<sub>4</sub> emissions from the Amazon basin, as observed by the airborne campaign TROPOZ II during the wet season, *J. Geophys. Res.*, 103, 19075–19091, <https://doi.org/10.1029/98JD01763>, 1998.
- Klippel, T., Fischer, H., Bozem, H., Lawrence, M. G., Butler, T., Jöckel, P., Tost, H., Martinez, M., Harder, H., Regelin, E., Sander, R., Schiller, C. L., Stickler, A., and Lelieveld, J.: Distribution of hydrogen peroxide and formaldehyde over Central Europe during the HOOVER project, *Atmos. Chem. Phys.*, 11, 4391–4410, <https://doi.org/10.5194/acp-11-4391-2011>, 2011.
- Lee, M., Heikes, B. G., and Jacob, D. J.: Enhancements of hydroperoxides and formaldehyde in biomass burning impacted air and their effect on atmospheric oxidant cycles, *J. Geophys. Res.*, 103, 13201–13212, <https://doi.org/10.1029/98JD00578>, 1998.
- Lelieveld, J. and Crutzen, P. J.: Role of deep cloud convection in the ozone budget of the troposphere, *Science*, 264, 1759–1761, <https://doi.org/10.1126/science.264.5166.1759>, 1994.
- Lelieveld, J., Gromov, S., Pozzer, A., and Taraborrelli, D.: Global tropospheric hydroxyl distribution, budget and reactivity, *Atmos. Chem. Phys.*, 16, 12477–12493, <https://doi.org/10.5194/acp-16-12477-2016>, 2016.
- Madronich, S. and Flocke, S.: The role of solar radiation in atmospheric chemistry, in *The Handbook of Environmental Chemistry Vol. 2 Part L Environmental Photochemistry*, edited by: P. Boule, Springer, Berlin, 1999.
- Marie, C., Jacob, D. J., and Bechtold, P.: Transport and scavenging of soluble gases in a deep convective cloud, *J. Geophys. Res.*, 105, 22255–22267, <https://doi.org/10.1029/2000JD900211>, 2000.
- Marie, C., Saut, C., Jacob, D. J., Staudt, A., Avery, M. A., Brune, W. H., Faloon, I., Heikes, B. G., Sachse, G. W., Sandholm, S. T., Singh, H. B., and Tan, D.: On the relative role of convection, chemistry, and transport over the South Pacific Convergence Zone during PEM-Tropics B: A case study, *J. Geophys. Res.*, 107, 8232, <https://doi.org/10.1029/2001JD001466>, 2002.
- Martinez, M., Harder, H., Kubistin, D., Rudolf, M., Bozem, H., Eerdeken, G., Fischer, H., Klüpfel, T., Gurk, C., Königstedt, R., Parchatka, U., Schiller, C. L., Stickler, A., Williams, J., and Lelieveld, J.: Hydroxyl radicals in the tropical troposphere over the Suriname rainforest: airborne measurements, *Atmos. Chem. Phys.*, 10, 3759–3773, <https://doi.org/10.5194/acp-10-3759-2010>, 2010.
- Pan, L., Homeyer, C. R., Honomichl, S., Ridley, B. A., Weisman, M., Barth, M. C., Hair, J. W., Fenn, M. A., Butler, C., Diskin, G. S., Crawford, J. H., Ryerson, T. B., Pollack, I., Peischl, J., and Huntrieser, H.: Thunderstorms enhance tropospheric ozone by wrapping and shedding stratospheric air, *Geophys. Res. Lett.*, 41, 7785–7790, <https://doi.org/10.1002/2014GL061921>, 2014.
- Pickering, K. E., Dickerson, R. R., Luke, W. T., and Nunnermacker, L. J.: Clear-sky vertical profiles of trace gases as influenced by upstream convective activity, *J. Geophys. Res.*, 94, 14879–14892, <https://doi.org/10.1029/JD094iD12p14879>, 1989.

- Pickering, K. E., Thompson, A. M., Wang, Y., Tao, W.-K., McNamara, D. P., Kirchhoff, V. W. J. H., Heikes, B. G., Sachse, G. W., Bradshaw, J. D., Gregory, G. L., and Blake, D. R.: Convective transport of biomass burning emissions over Brazil during TRACE A, *J. Geophys. Res.*, 101, 23993–24012, <https://doi.org/10.1029/96JD00346>, 1996.
- Poulida, O., Dickerson, R. R., and Heymsfield, A.: Stratosphere-troposphere exchange in a midlatitude mesoscale convective complex: 1. Observations, *J. Geophys. Res.*, 101, 6823–6836, <https://doi.org/10.1029/95JD03523>, 1996.
- Pöschl, U., von Kuhlmann, R., Posson, N., and Crutzen, P. J.: Development and intercomparison of condensed isoprene oxidation mechanisms for global atmospheric modeling, *J. Atmos. Chem.*, 37, 29–52, <https://doi.org/10.1023/A:1006391009798>, 2000.
- Prather, M. J. and Jacob, D. J.: A persistent imbalance in HO<sub>x</sub> and NO<sub>x</sub> photochemistry of the upper troposphere driven by deep convection, *Geophys. Res. Lett.*, 24, 3189–3192, <https://doi.org/10.1029/97GL03027>, 1997.
- Regelin, E., Harder, H., Martinez, M., Kubistin, D., Tatum Ernest, C., Bozem, H., Klippel, T., Hosaynali-Beygi, Z., Fischer, H., Sander, R., Jöckel, P., Königstedt, R., and Lelieveld, J.: HO<sub>x</sub> measurements in the summertime upper troposphere over Europe: a comparison of observations to a box model and a 3-D model, *Atmos. Chem. Phys.*, 13, 10703–10720, <https://doi.org/10.5194/acp-13-10703-2013>, 2013.
- Ren, Y., Baumann, R., and Schlager, H.: An airborne perfluorocarbon tracer system and its first application for a Lagrangian experiment, *Atmos. Meas. Tech.*, 8, 69–80, <https://doi.org/10.5194/amt-8-69-2015>, 2015.
- Ridley, B., Ott, L., Pickering, K., Emmons, L., Montzka, D., Weinheimer, A., Knapp, D., Grahek, F., Li, L., Heymsfield, G., McGill, M., Kucera, P., Mahoney, M. J., Baumgardner, D., Schultz, M., and Brasseur, G.: Florida thunderstorms: A faucet of reactive nitrogen to the upper troposphere, *J. Geophys. Res.*, 109, D17305, <https://doi.org/10.1029/2004JD004769>, 2004.
- Sander, R., Kerkweg, A., Jöckel, P., and Lelieveld, J.: Technical note: The new comprehensive atmospheric chemistry module MECCA, *Atmos. Chem. Phys.*, 5, 445–450, <https://doi.org/10.5194/acp-5-445-2005>, 2005.
- Sandu, A. and Sander, R.: Technical note: Simulating chemical systems in Fortran90 and Matlab with the Kinetic PreProcessor KPP-2.1, *Atmos. Chem. Phys.*, 6, 187–195, <https://doi.org/10.5194/acp-6-187-2006>, 2006.
- Scala, J. R., Garstang, M., Tao, W.-K., Pickering, K. E., Thompson, A. M., Simpson, J., Kirchhoff, V. W. J. H., Browell, E. V., Sachse, G. W., Torres, A. L., Gregory, G. L., Rasmussen, R. A., and Khalil, M. A. K.: Cloud draft structure and trace gas transport, *J. Geophys. Res.*, 95, 17015–17030, <https://doi.org/10.1029/JD095iD10p17015>, 1990.
- Schiller, C. L., Bozem, H., Gurk, C., Parchatka, U., Königstedt, R., Harris, G. W., Lelieveld, J., and Fischer, H.: Applications of quantum cascade lasers for sensitive trace gas measurements of CO, CH<sub>4</sub>, N<sub>2</sub>O, and HCHO, *Appl. Phys.*, B92, 419–430, <https://doi.org/10.1007/s00340-008-3125-0>, 2008.
- Snider, J. R., Montague, D. C., and Vali, G.: Hydrogen peroxide retention in rime ice, *J. Geophys. Res.*, 97, 7569–7578, <https://doi.org/10.1029/92JD00237>, 1992.
- Snider, J. R. and Huang, J.: Factors influencing the retention of hydrogen peroxide and molecular oxygen in rime ice, *J. Geophys. Res.*, 103, 1405–1415, <https://doi.org/10.1029/97JD02847>, 1998.
- Stickler, A., Fischer, H., Williams, J., de Reus, M., Sander, R., Lawrence, M. G., Crowley, J. N., and Lelieveld, J.: Influence of summertime deep convection on formaldehyde in the middle and upper troposphere over Europe, *J. Geophys. Res.*, 111, D14308, <https://doi.org/10.1029/2005JD007001>, 2006.
- Ström, J., Fischer, H., Lelieveld, J., and Schröder, F.: In situ measurements of microphysical properties and trace gases in two cumulonimbus anvils over western Europe, *J. Geophys. Res.*, 104, 12221–12226, <https://doi.org/10.1029/1999JD900188>, 1999.
- von Blohn, N., Diehl, K., Mitra, S. K., and Borrmann, S.: Wind tunnel experiments on the retention of trace gases during riming: nitric acid, hydrochloric acid, and hydrogen peroxide, *Atmos. Chem. Phys.*, 11, 11569–11579, <https://doi.org/10.5194/acp-11-11569-2011>, 2011.
- Wang, C. and Crutzen, P. J.: Impact of a simulated severe local storm on the redistribution of sulfur dioxide, *J. Geophys. Res.*, 100, 11357–11367, <https://doi.org/10.1029/95JD00697>, 1995.
- Wang, C. and Prinn, R. G.: On the roles of deep convective clouds in tropospheric chemistry, *J. Geophys. Res.*, 105, 22269–22297, <https://doi.org/10.1029/2000JD900263>, 2000.
- Yin, Y., Carslaw, K. S., and Parker, D. J.: Redistribution of trace gases by convective clouds – mixed-phase processes, *Atmos. Chem. Phys.*, 2, 293–306, <https://doi.org/10.5194/acp-2-293-2002>, 2002.